ARTICLE

Hierarchical Organization and Catalytic Activity of High-Surface-Area Mesoporous Ceria Microspheres Prepared Via Hydrothermal Routes

Hongfeng Li, Guanzhong Lu,* Qiguang Dai, Yanqin Wang, Yun Guo, and Yanglong Guo

Key Laboratory for Advanced Materials and Research Institute of Industrial Catalysis, East China University of Science and Technology, Shanghai 200237, P. R. China

ABSTRACT Mesoporous $Ce(OH)CO_3$ microspheres with flowerlike three-dimensional (3D) hierarchical structure were successfully synthesized via different hydrothermal systems, including glucose/acrylic acid, fructose/acrylic acid, glucose/propanoic acid, and glucose/*n*-butylamine systems. After $Ce(OH)CO_3$ microspheres were calcined, mesoporous CeO_2 microspheres with the same flowerlike morphology as $Ce(OH)CO_3$ microspheres were obtained. Especially, flowerlike CeO_2 microspheres prepared via the glucose/acrylic acid system are composed of many interconnected mesoporous petal-like nanosheets with thicknesses of 40−60 nm and have high surface area (211 $m^2\ g^{-1}$), large pore volume (0.32 $cm^3\ g^{-1}$), and narrow pore size distribution (~3.8 nm in diameter). A possible formation mechanism of $Ce(OH)CO_3$ microspheres is proposed: the large N-containing organic compounds in situ produced in the above reaction systems played a crucial role in controlling the assembly of $Ce(OH)CO_3$ building blocks into the flowerlike $Ce(OH)CO_3$ microspheres. For trichloroethylene combustion, flowerlike CeO_2 microspheres were found to exhibit much higher catalytic activity than general CeO_2 prepared with the conventional methods and the $T_{10\%}$ and $T_{90\%}$ were as low as 100 and 204 °C, respectively.

KEYWORDS: mesoporous CeO_2 microsphere • flowerlike morphology • high surface area • catalytic activity • trichloroethylene combustion

1. INTRODUCTION

As one of the most important rare-earth oxides, ceria has attracted much attention recently, because of its extensive roles in various fields, such as the promoters for three-way catalysts (TWCs) (1, 2), fuel cells (3), oxygen sensors (4), phosphors (5), polishing materials (6), and hydrogen storage materials (7). Although the intrinsic chemical properties of ceria, such as high oxygen storage capacity (OSC) and high oxygen mobility, both of which originate from facile Ce^{3+}/Ce^{4+} redox cycle, dominate its utilization, its different structures and morphologies have also been proved to have a significant influence on its properties and further on its applications (8, 9). So far, ceria with various structures and morphologies such as mesoporous structures (10), nanowires (11), nanorods (12), nanotubes (13), nanocubes (14), nanopolyhedra (15), and nanoflowers (16) have been reported in the last decades. The size/structure/morphology-dependent properties of ceria were investigated and confirmed that its novel functions are distinguishable compared with general ceria. For example, mesoporous ceria has apparent advantages in enhancing the catalytic activities, because the mesostructures not only possess high surface area for facilitating dispersion of other active components when ceria is used as a support, but also can favor transportation of reactant molecules to the active sites more effectively (17). Ceria nanotubes prepared under low temperature by an oxidation-coordination-assisted dissolution process of cerium hydroxide precursors showed a high oxygen storage capacity because of their larger cavities and thin walls (18). Dimension-tunable ceria nanostructures could be selectively synthesized from the same cerium precursor of $Ce(OC_8H_{17})_4$ with the designed solution methods. It was found that polycrystalline assembled nanostructure catalyst and nanopolyhedra catalyst exhibited higher activities for CO oxidation than mesoporous catalyst, because of the higher particle dispersity of the former two than that of the latter (19). Recently, a variety of chemical techniques have been intentionally explored to fabricate ceria with various structures and morphologies, including a hydrothermal/solvothermal process (20), spray pyrolysis (21), microemulsion (22), sonochemical route (23), template-assisted synthesis (24), template-free synthesis (25), and so on. Among these preparation techniques, the hydrothermal/solvothermal-based process (may be assisted by other additives or templates) is one of the most effective approaches for preparing the materials with desirable structures and morphologies.

In the past few years, three-dimensional (3D) micro/nanocomposite materials derived from assembly of nanoscale building blocks have considerably inspired the researchers' enthusiasms, because of their hierarchical architectures with unique properties and novel functionalities (26, 27). Likewise, some efforts were devoted to a fabrication

* Corresponding Author: Guanzhong Lu, Tel: +86-21-64252923. Fax: +86-21-64253703. E-mail: gzhlu@ecust.edu.cn.

Received for review November 25, 2009 and accepted February 22, 2010

DOI: 10.1021/am900829y

Published on Web 03/05/2010

of ceria with 3D hierarchical architecture (28–30). However, their relative low surface areas are still a non-negligible drawback, especially when ceria is used in catalysis field. For instance, porous hollow microspheres of ceria could be prepared via a simple carbon microsphere template method and had the surface area up to 144.1 $m^2 g^{-1}$ (30). Although the surface area is higher than general ceria, extensive usage of these ceria microspheres is still limited if they are used as effective catalyst materials. Therefore, it is still a challenge to exploit 3D hierarchical structured mesoporous ceria with a high surface area.

Herein, several synthesis systems, such as glucose/acrylic acid, fructose/acrylic acid, glucose/propanoic acid, and glucose/*n*-butylamine systems, have been respectively adopted to synthesize flowerlike $Ce(OH)CO_3$ microspheres with unique 3D hierarchical structure. Upon calcination of these $Ce(OH)CO_3$ microspheres, mesoporous CeO_2 microspheres with high surface area and same flower-like morphology were thus attained. A possible mechanism is proposed that it was not the graft copolymers but the in situ produced large N-containing organic compounds to control the assembly of $Ce(OH)CO_3$ building blocks into flowerlike $Ce(OH)CO_3$ microspheres, since neither propanoic acid nor *n*-butylamine is vinyl monomer like acrylic acid and their graft copolymerizations onto glucose could not occur in either glucose/propanoic acid or glucose/n-butylamine systems (31, 32), which was different from the cases in glucose/acrylic acid or fructose/acrylic acid systems.

Recently, we have found that CeO_2 prepared by calcination of $Ce(NO_3)_3 \cdot 6H_2O$ had a high catalytic activity for the combustion of trichloroethylene (33), which is one of chlorinated volatile organic compounds (CVOCs) that are harmful to human health and ecological environment (34, 35). Using the catalytic destruction of trichloroethylene as a model reaction, the flowerlike CeO_2 microspheres were found to show much higher activity than general CeO_2 prepared by the direct calcination or precipitation method from hexahydrated cerium nitrate.

2. EXPERIMENTAL SECTION

2.1. Synthesis of Flowerlike $Ce(OH)CO_3$ Microspheres. ***(1) Glucose/Acrylic Acid System.*** All chemicals (Sinopharm Chemical Reagent Co., Ltd., except for acrylic acid provided by Shanghai Chemical Reagent Co., Ltd.) were used without further purification. Typically, glucose (0.01 mol) and acrylic acid (0.015 mol) were dissolved into deionized water (80 mL) under magnetic stirring, followed by adding $Ce(NO_3)_3 \cdot 6H_2O$ (0.005 mol) to form a transparent solution, and then ammonia solution (4.4 mL, 25 wt %) was added to this solution dropwise. The pH value of this resultant gel was ~10. After being stirred at 30 °C for 5 h, this brown gel was transferred into a Teflon-lined autoclave (100 mL), and then sealed and kept at 180 °C for 72 h in an electric oven. After the autoclave was cooled down to room temperature naturally, the orange solid precipitate was collected by filtration, alternately washed with deionized water and alcohol six times, and then dried at 80 °C overnight. Finally, flowerlike $Ce(OH)CO_3$ microspheres were obtained.

(2) Fructose/Acrylic Acid, Glucose/Propanoic Acid, and Glucose/n-Butylamine Systems. When the fructose/acrylic acid, glucose/propanoic acid, and glucose/*n*-butylamine systems were used to synthesize flowerlike $Ce(OH)CO_3$ microspheres, the hydrothermal temperatures were all raised to 200 °C and the amount of ammonia solution is 3.4 mL for just the glucose/*n*-butylamine system. Other conditions were the same as in part 1 above.

2.2. Preparation of Flowerlike CeO_2 Microspheres. The flowerlike CeO_2 micropheres were obtained from the as-synthesized $Ce(OH)CO_3$ microspheres by two-step calcinations: they were first calcined at 600 °C for 6 h in N_2 (10 mL min^{-1}, kept at room temperature for 30 min prior to heating) in the tube furnace and then calcined at 400 °C for 4 h in air. This special calcination process was adopted to avoid acute decomposition of $Ce(OH)CO_3$ micropheres in air. The flowerlike CeO_2 microspheres prepared in the glucose/acrylic acid system were denoted as CeO_2-F. For comparison, the reference CeO_2 obtained by the direct calcination of $Ce(NO_3)_3 \cdot 6H_2O$ at different temperatures for 6 h in air was denoted as CeO_2(*T*)-D, in which *T* is the calcination temperature. Likewise, another reference CeO_2 prepared by the precipitation of $Ce(NO_3)_3 \cdot 6H_2O$ solution with ammonia and calcined at different temperatures for 6 h in air was denoted as CeO_2(*T*)-P.

2.3. Characterization. Power X-ray diffraction patterns were performed on a Rigaku D/max 2250 VB/PC diffractometer with CuKα radiation (λ =1.5406 Å; 40 kV, 100 mA, scanning step = 0.02°). The average crystalline size was calculated by the Scherrer formula with a Scherrer constant of 0.89. Transmission electron microscope (TEM) images and scanning electron microscope (SEM) images were obtained on a TECNAI 20S-TWIN and JSM-6360LV, respectively. N_2 adsorption−desorption isotherms were measured at 77 K on a NOVA 4200e surface area & pore size analyzer. Before measurement, all samples were outgassed in vacuum at 300 °C for 4 h except $Ce(OH)CO_3$ microspheres were outgassed in a vacuum at 100 °C for 12 h. The Brunauer−Emmett−Teller (BET) method was used to calculate the surface areas of samples. The pore size distributions were derived from the desorption branches of the isotherms using the Barrett−Joyner−Halanda (BJH) method. The total pore volume was estimated at a relative pressure of 0.985. Hydrogen temperature-programmed reductions (H_2-TPR) of the samples were carried out in a conventional flow system equipped with a thermal conductivity detector (TCD). A 50 mg sample was used and pretreated in a 5 % O_2/N_2 flow (40 mL min^{-1}) at 400 °C for 30 min prior to run. After the sample was cooled to room temperature, a 5 % H_2/N_2 mixture gas (40 mL min^{-1}) was introduced and the reactor was heated at a rate of 10 °C min^{-1} from room temperature to ~800 °C. Reduction of CuO to metal Cu was used to calibrate the hydrogen consumption. The element analyses of the samples were carried out with the energy-dispersive X-ray spectrum (EDS) detector (EDAX, FALCON).

2.4. Catalytic Activity Testing for Trichloroethylene Combustion. The activities of catalysts were carried out in a continuous flow microreactor consisted of a U-shaped quartz tube (Ø 4 mm, inner diameter) at atmospheric pressure. Two-hundred milligrams of catalyst was packed at the bottom of the reactor. The feed flow through the reactor was 50 cm^3 min^{-1} and the gas hourly space velocity (GHSV) was 15 000 h^{-1}. Feed gas was prepared by delivering liquid trichloroethylene with a syringe pump into dry air controlled by a mass flow controller, in which the injection point was electrically heated to ensure complete evaporation of trichloroethylene. The concentration of trichloroethylene in the feed gas was 1000 ppm. The effluent gas was analyzed online by two gas chromatographs (GC), one equipped with an electron capture detector (ECD) to analyze quantitatively the organic chlorinated compounds and the other with a thermal conductivity detector (TCD) to analyze quantitatively CO and CO_2. The concentrations of Cl_2 and HCl were analyzed by the effluent gas bubbling through a 0.0125N NaOH solution. Then the Cl_2 concentration was determined by titration with ferrous ammonium sulfate (FAS) in *N*,*N*-diethyl-*p*-phenylenedi-

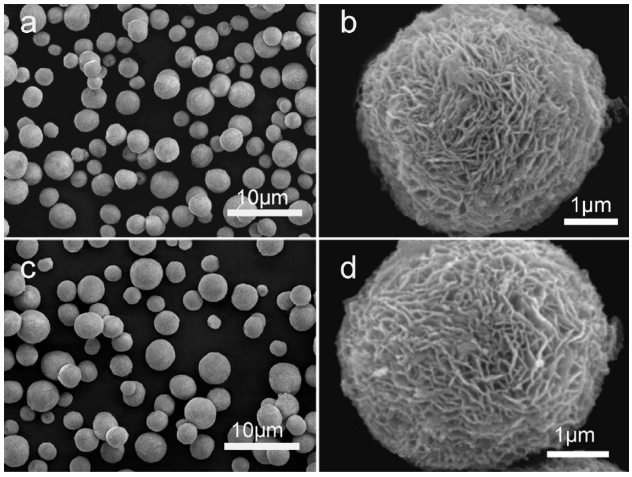

FIGURE 1. SEM images of (a, b) flowerlike $Ce(OH)CO_3$ microspheres and (c, d) flowerlike CeO_2 microspheres as-prepared in glucose/acrylic acid system.

amine (DPD) as an indicator (36). The concentration of chloride ions in the bubbled solution was determined using a chloride ion selective electrode (37).

3. RESULTS AND DISCUSSION

3.1. Flowerlike $Ce(OH)CO_3$ and CeO_2 Microspheres Prepared in the Glucose/Acrylic Acid System. The SEM images of as-synthesized $Ce(OH)CO_3$ microspheres in glucose/acrylic acid system and their calcined products CeO_2 microspheres are exhibited in Figure 1. It can be seen from Figure 1a that as-synthesized monodisperse $Ce(OH)CO_3$ microspheres have the diameters of 2−5 μm. Figure 1b shows a beautiful flowerlike microsphere consisting of a large number of petal-like nanosheets with thicknesses of 40−60 nm, and these nanosheets interweave together to form an open porous structure. After the calcination of $Ce(OH)CO_3$ microspheres, flowerlike CeO_2 microspheres were obtained with the similar morphologies and sizes as their parents (Figure 1c,d).

The TEM images of flowerlike CeO_2 microspheres are shown in Figure 2. Figure 2a shows that monodisperse CeO_2 microspheres have the diameters ranging from 2 to 5 μm, in agreement with SEM results. Figure 2b clearly indicates that CeO_2 microsphere has a hollow structure. Figure 2c is the high-resolution TEM image of the edged part of a petal-like nanosheet of the CeO_2 microspheres, which shows that the worm-like mesopores with pore sizes of 2−5 nm spread over the nanosheet. The selected area electron diffraction (SAED) pattern (Figure 2c, inset) indicates the structure of the microspheres is a face-centered cubic CeO_2. Two interplanar spacings of the ordered stripes marked in Figure 2d are ~0.31 and ~0.27 nm, corresponding to the (111) and (200) lattice planes of CeO_2, respectively. These nanocrystals have a random orientation, also indicating a polycrystalline characteristic (28). An average size of nanocrystals observed from different orientations is ~6 nm.

The XRD patterns in Figure 3 show that $Ce(OH)CO_3$ microspheres exist as a hexagonal phase (JCPDS file 32−0189) and CeO_2 microspheres as a face-centered cubic phase (JCPDS file 34−0394), which is in accord with the SAED

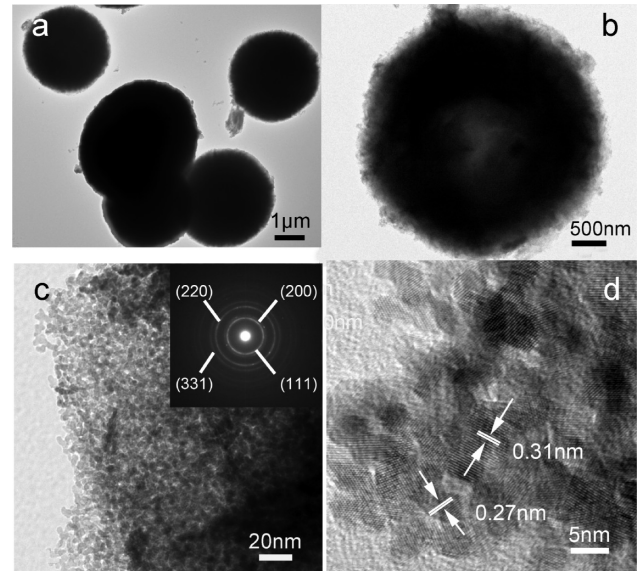

FIGURE 2. TEM images of CeO_2 microspheres: (a) an overall view of CeO_2 microspheres; (b) detailed view on an individual microsphere; (c, d) HRTEM images of one nanosheet on CeO_2 microspheres and (c, inset) a SAED pattern.

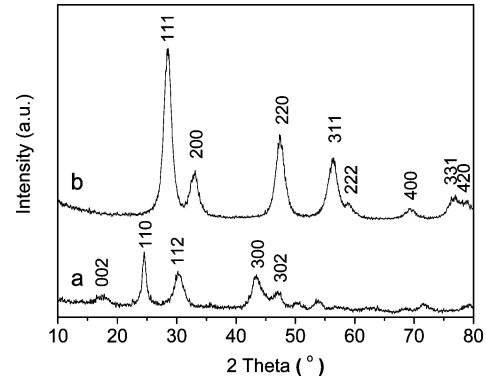

FIGURE 3. XRD patterns of (a) $Ce(OH)CO_3$ (hexagonal phase, JCPDS file 32−0189) and (b) CeO_2 microspheres (face centered cubic phase, JCPDS file 34−0394).

pattern. Their average grain sizes calculated by the Scherrer equation are ~7.1 and ~6.5 nm, respectively. The latter is consistent with that observed in the HRTEM image.

The nitrogen adsorption−desorption isotherm of flowerlike $Ce(OH)CO_3$ microspheres exhibits the type-IV curve with a H3-type hysteresis loop (Figure 4a). It need be noted that the adsorption−desorption isotherms are not closed in the low relative pressure region, suggesting there still exist some large organic remnants in the form of networks inside petal-like nanosheets of flowerlike $Ce(OH)CO_3$ microspheres, though the in situ produced graft copolymers from glucose and acrylic acid had been mostly decomposed in basic solution during the hydrothermal reaction and $Ce(OH)CO_3$ microspheres had been washed as well. These organic networks would relax and swell in condensed liquid nitrogen at high relative pressures during the test, so the pore volume inside organic networks correspondingly augmented, leading to larger desorption pore volume than the adsorption pore volume even in the low relative pressure region (38, 39). The $Ce(OH)CO_3$ microspheres have a narrow pore size distribution centered at ~3.9 nm (Figure 4a, inset), and their

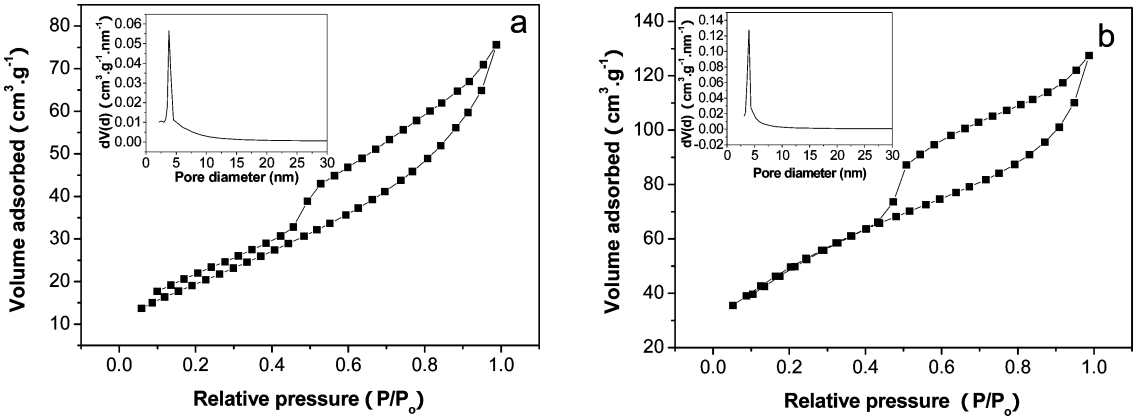

FIGURE 4. Nitrogen adsorption−desorption isotherms and the BJH pore distribution curves of (a) $Ce(OH)CO_3$ and (b) CeO_2 microspheres.

Table 1. Effects of Aging Temperatures of Gel Prior to Hydrothermal Reactions in Glucose/Acrylic Acid System on the Textural Properties of Flowerlike CeO_2 Microspheres

T (°C)	surface area (m^2 g^{-1})[a]	pore volume (cm^3 g^{-1})[a]	pore diameter (nm)[a]
0	211.0	0.32	3.8
10	194.8	0.26	3.8
20	202.3	0.19	3.7
30	181.4 (131.2)	0.20 (0.17)	3.9 (3.8)
40	152.2	0.17	3.6
50	138.5	0.15	3.6

[a] The values in parentheses were obtained from flowerlike CeO_2 microspheres calcined directly in air at 400 °C for 4 h.

BET surface area and pore volume are 75.8 m^2 g^{-1} and 0.14 cm^3 g^{-1}, respectively. After calcination, the obtained CeO_2 microspheres also possess the type IV adsorption−desorption isotherm with a H4-type hysteresis loop and well-defined uniform pore sizes of ~3.9 nm (Figure 4b and inset). Their BET surface area reaches 181.4 m^2 g^{-1} and the pore volume is 0.20 cm^3 g^{-1}. However, as $Ce(OH)CO_3$ microspheres were directly calcined in air at 400 °C for 4 h, the BET surface area of obtained CeO_2 microspheres is decreased to only 131.2 m^2 g^{-1} (Table 1), suggesting that their mesoporous structure has been partially destroyed.

3.2. Effects of Synthesis Conditions on the Properties of Flowerlike CeO_2 Microspheres. It is found that the BET surface areas of flower-like CeO_2 microspheres were obviously affected by the aging temperatures of the gel prior to hydrothermal reactions (Table 1). The results show that the relative low aging temperature was favorable for increasing the BET surface area and pore volume of flowerlike CeO_2 microspheres. For instance, when the aging temperature declined to 0 °C, the BET surface area and pore volume of flowerlike CeO_2 microspheres were increased to 211 m^2 g^{-1} and 0.32 cm^3 g^{-1}, respectively. It was possible that the graft-copolymerization reaction between glucose and acrylic acid occurred more easily at lower temperatures, and after the decomposition of these graft copolymers more and larger organic compounds were produced, which were embedded in petal-like nanosheets

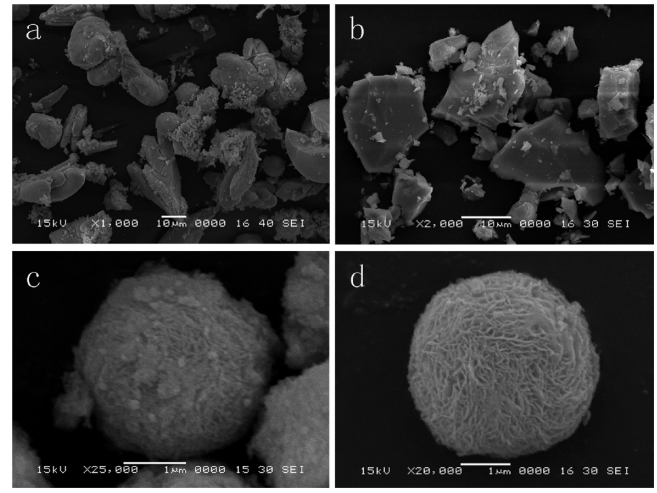

FIGURE 5. SEM images of morphology evolution of $Ce(OH)CO_3$ microspheres with various hydrothermal reaction stages: (a) 0, (b) 24, (c) 48, and (d) 72 h.

and enhanced pore production of CeO_2 microspheres after thermal treatment. More details will be discussed in the later section.

To reveal the evolution process of morphology of $Ce(OH)CO_3$ microspheres, the samples collected in different stages of the hydrothermal reaction were investigated by SEM. As shown in Figure 5a, the sample aged at 30 °C for 5 h without hydrothermal treatment shows large loosely aggregated bulks. After hydrothermal reaction for 24 h, the bulks became dense and smooth (Figure 5b). As the hydrothermal time was prolonged to 48 h, rough flowerlike $Ce(OH)CO_3$ microspheres can be observed (Figure 5c), and after 72 h, perfect flowerlike $Ce(OH)CO_3$ microspheres were achieved (Figure 5d). Figure 6 shows the XRD patterns of the above four samples. No diffraction peaks are observed even if the hydrothermal time was prolonged to 24 h, that is, the sample in this period was very poorly crystallized or in amorphous state. After hydrothermal reaction for 48 h, the diffraction peaks have appeared that are mainly assigned to hexagonal phase of $Ce(OH)CO_3$ with a very small amount of orthorhombic phase. Seventy-two hours later, a highly crystalline $Ce(OH)CO_3$ with the complete hexagonal phase was obtained.

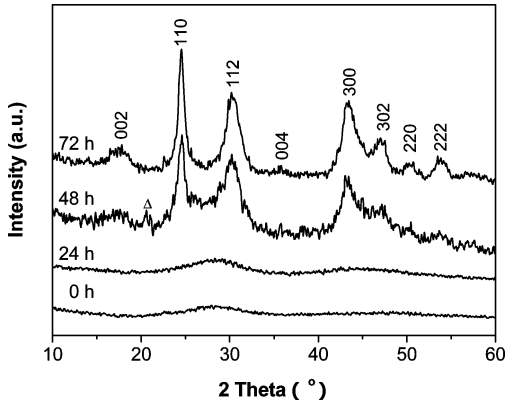

FIGURE 6. XRD patterns of as-synthesized products with different reaction times: (a) 0, (b) 24, (c) 48, and (d) 72 h. (The peaks indexed are assigned to hexagonal phase of $Ce(OH)CO_3$ and the Δ peak is assigned to orthorhombic phase (JCPDS file 41−0013).

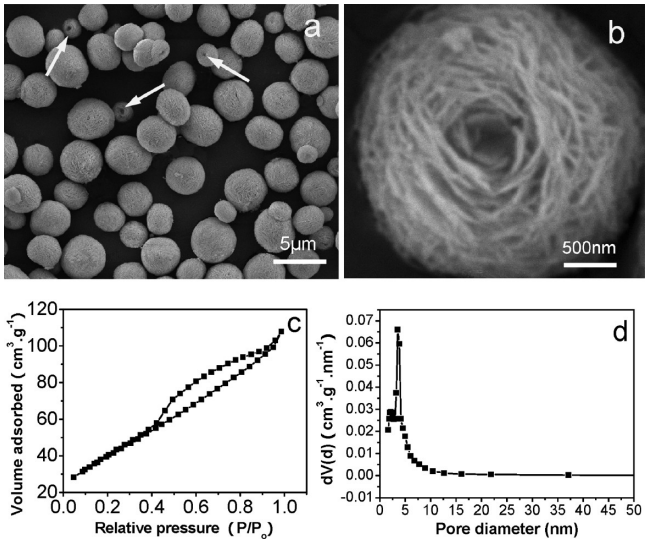

FIGURE 7. SEM images of flowerlike CeO_2 microspheres prepared in the fructose/acrylic acid system: (a) an overall view of microspheres; (b) a representative image of the microsphere with exposed hollow structure; (c) their N_2 adsorption/desorption isotherm; and (d) corresponding pore size distribution.

3.3. Flowerlike $Ce(OH)CO_3$ and CeO_2 Microspheres Prepared in the Fructose/Acrylic Acid, Glucose/Propanoic Acid, and Glucose/*n*-Butylamine Systems, Respectively. Flowerlike CeO_2 microspheres prepared in the fructose/acrylic acid system are displayed in Figure 7. These CeO_2 microspheres have the diameters of 2−5 μm and the thicknesses of nanosheets as petals are 50−70 nm. Some relatively small microspheres pointed at with the arrows clearly present a spirally/radially grown hollow structure, just like the bird's nests. The detail view of one individual microsphere is presented in Figure 7b. In fact, this kind of exposed hollow microsphere can also be found when prepared in glucose/acrylic acid system (see Figure S1 in the Supporting Information). Figure 7c shows a type IV isotherm with H4-type hysteresis loop and well-defined uniform mesopore sizes of ∼3.7 nm. Their BET surface area and BJH desorption cumulative pore volume are 146 $m^2 g^{-1}$ and 0.17 $cm^3 g^{-1}$, respectively.

Flowerlike $Ce(OH)CO_3$ microspheres could also be prepared in the glucose/propanoic acid system. XRD patterns reveal they are main hexagonal phase $Ce(OH)CO_3$, along with a small amount of orthorhombic phase $Ce(OH)CO_3$ (see Figure S2 in the Supporting Information). However, these hydrothermal products exhibit dark color, differing from the general orange ones. Figure 8a shows the SEM image of one $Ce(OH)CO_3$ microsphere that is attached by some carbon particles produced in pyrolysis of some glucose. After calcination, the attached carbon particles were combusted and the corresponding CeO_2 microsphere was obtained with clearly perfect flower-like morphology (Figure 8b). Its size is ∼9 μm and the thicknesses of the interconnected nanosheets are in the range of 50−80 nm. Figure 8c shows a type IV adsorption−desorption isotherm with a H4-type hysteresis loop, and a sharp pore size distribution curve centered at ∼3.9 nm (Figure 8c, inset), demonstrating the uniform mesopores. Its BET surface area and pore volume are 84 $m^2 g^{-1}$ and 0.16 $cm^3 g^{-1}$, respectively. When the glucose/*n*-butylamine system was adopted, flowerlike CeO_2 microspheres with diameters of 2−5 μm could be prepared as well (Figure 9).

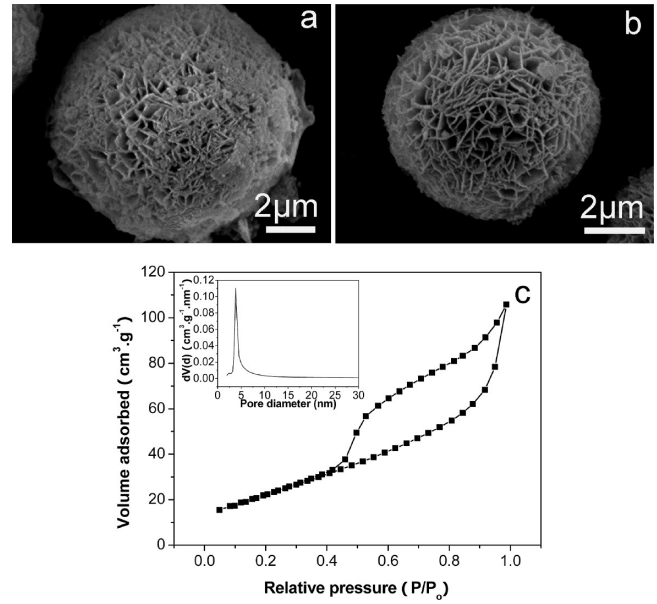

FIGURE 8. SEM images of (a) flowerlike $Ce(OH)CO_3$ and (b) CeO_2 microspheres prepared in glucose/propanoic acid system, and (c) N_2 adsorption−desorption isotherm and pore size distribution curve (inset) of CeO_2 microspheres.

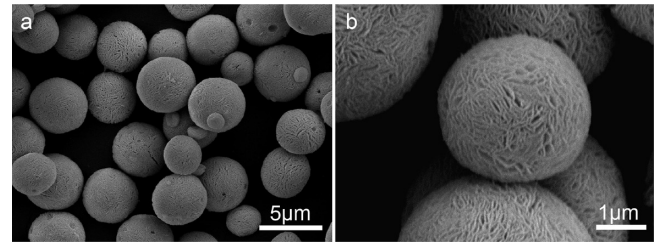

FIGURE 9. SEM images of flowerlike CeO_2 microspheres prepared in the glucose/*n*-butlyamine system.

3.4. Discussion for the Possible Formation Mechanism of Flowerlike $Ce(OH)CO_3$ Microspheres. During the synthesis processes of flowerlike $Ce(OH)CO_3$ microspheres in the glucose/acrylic acid or fructose/acrylic acid system, acrylic acid could be graft-copolymerized onto

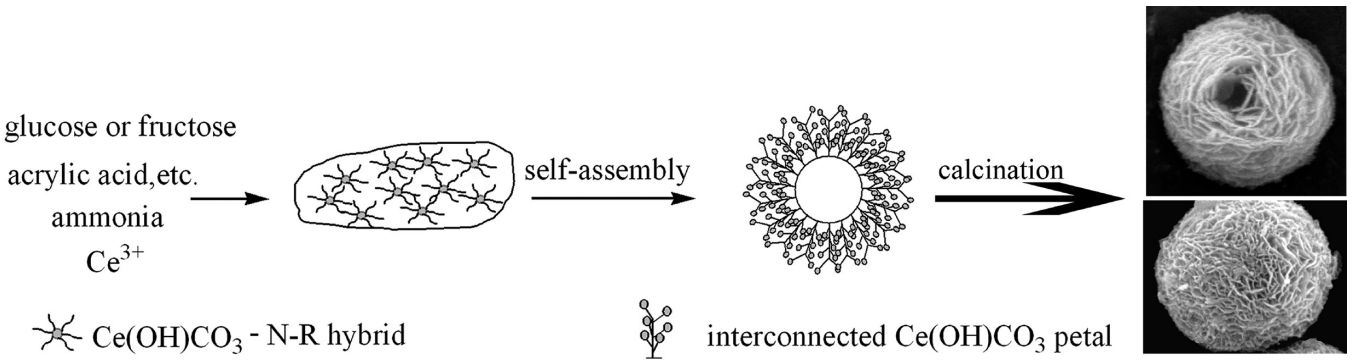

FIGURE 10. Schematic illustration of the formation evolution of flowerlike CeO_2 microspheres.

glucose or fructose to form graft-copolymers (31, 32). However, under hydrothermal conditions, these graft copolymers in the basic solution were easily decomposed (40, 41), which could be testified by GC-MS analysis of organic products collected just after hydrothermal reaction in the glucose/acrylic acid system (see Figure S3a in the Supporting Information). It shows that many various large N-containing organic compounds were produced in the hydrothermal reaction. Besides decomposition of graft copolymers, ammonolysis of $-COOH$ in ammonia solution and subsequent decarbonylation of $-CONH_2$ catalyzed by base (42), dehydration between amine and $-OH$, and other complex reactions might be responsible for the formation of these N-containing organic compounds.

When the glucose/propanoic acid system was adopted, flowerlike $Ce(OH)CO_3$ microspheres could also be obtained. It is worth noting that there were no graft-copolymers produced because it is impossible that graft copolymerization can take place between glucose and propanoic acid, due to the absence of vinyl groups for free-radical polymerization. But N-containing organic compounds could still be produced in ammonia solution through the complex reactions, such as ammonolysis, decarbonylation, alkaline degradation, dehydration, etc. These N-containing organic compounds were also confirmed by the GC-MS analysis (see Figure S3b in the Supporting Information) and the absence of more and larger N-containing organic compounds suggests that there were no graft copolymers produced. Likewise, graft-copolymerzation cannot occur between glucose and *n*-butylamine, but flowerlike $Ce(OH)CO_3$ microspheres could also be produced in the glucose/*n*-butylamine system.

If only glucose was adopted, only a small number of aggregated spherelike $Ce(OH)CO_3$ without flowerlike structures can be observed. If glucose was absent, bulk CeO_2 instead of $Ce(OH)CO_3$ microspheres was obtained, because glucose could supply CO_3^{2-} ions by its degradation in base solution (40), and furthermore, glucose could act as the reducing agent and hinder the oxidation of $Ce(OH)_3$ into $Ce(OH)_4$ by air in base solution. If maltose and acrylic acid were adopted and other synthesis conditions were the same as those in the glucose/acrylic system, flowerlike $Ce(OH)CO_3$ microspheres could not be obtained either. Therefore, it can be inferred that the formation of flowerlike $Ce(OH)CO_3$ microspheres was not relative to glucose self-polymerization by dehydration between $-OH$, because maltose is just the glycosidation product of two glucose molecules.

On the basis of the above results, we can conclude that it was not graft-copolymers but the in situ produced N-containing organic compounds to control the formation of flowerlike $Ce(OH)CO_3$ microspheres. The roles of the N-containing organic compounds could also be further confirmed by the fact that if NaOH solution instead of ammonia solution was used, no flowerlike $Ce(OH)CO_3$ microspheres could be achieved in glucose/acrylic acid system, because no nitrogen source could be supplied in the whole reaction system to form N-containing organic compounds. Therefore, a possible mechanism is proposed that the in situ produced N-containing organic compounds interacted with $Ce(OH)CO_3$ particles to form $Ce(OH)CO_3-N-R$ hybrids, which then self-assemblied as building blocks into flowerlike $Ce(OH)CO_3$ microspheres (43, 44), as schematically described in Figure 10. It should be noted that the flowerlike CeO_2 microspheres prepared in the glucose/propanoic acid or glucose/*n*-butlyamine systems have the relative low BET surface areas ($<90\ m^2\ g^{-1}$). This may be attributed to no formation of graft-copolymers in above synthesis systems, resulting in the scarcity of larger N-containing organic compounds produced from graft-copolymers, which promoted the formation of mesopores inside petal-like nanosheets of flowerlike CeO_2 microspheres. Furthermore, it seems that, to some extent, the more and larger the in situ produced N-containing organic compounds, the more easily flowerlike $Ce(OH)CO_3$ microspheres could be produced. This is the reason why the hydrothermal synthesis temperature should be increased from 180 °C for the glucose/acrylic acid system to 200 °C for the glucose/propanoic acid or glucose/*n*-butlyamine system, in order to obtain perfect flowerlike $Ce(OH)CO_3$ microspheres.

3.5. Catalytic Performance of Flowerlike CeO_2 Microspheres for Trichloroethylene Combustion. Trichloroethylene combustion was carried out for investigating catalytic activity of flowerlike CeO_2 microspheres (CeO_2-F) prepared in glucose/acrylic acid system. As shown in Figure 11, flowerlike CeO_2 microspheres show an excellent activity for the trichloroethylene elimination. The ignition temperature $T_{10\%}$ (the reaction temperature at 10% conversion) is only 100 °C and $T_{90\%}$ (the reaction temperature at 90% conversion) is as low as 204 °C.

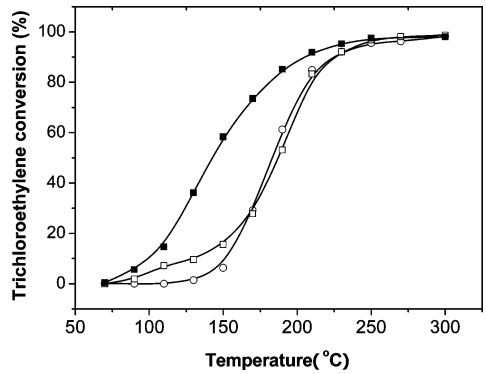

FIGURE 11. Light-off curves for catalytic combustion of trichloroethylene over (■) CeO_2-F, (□) CeO_2 (500)-D, and (○) CeO_2 (500)-P.

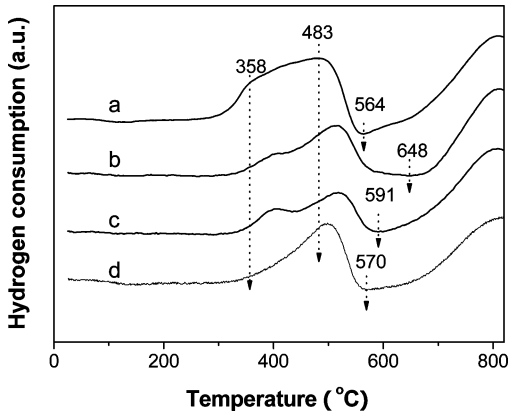

FIGURE 12. H_2-TPR curves of (a) CeO_2-F, (b) CeO_2 (500)-D, (c) CeO_2 (500)-P, and (d) used CeO_2-F.

For comparison, bulk CeO_2-D prepared by direct calcination of $Ce(NO_3)_3 \cdot 6H_2O$ in air for 6 h at 400, 500, 600 °C, respectively and CeO_2—P obtained by a precipitation method with ammonia precipitant followed by calcinations in the same conditions as CeO_2-D were used as the reference catalysts. It is discovered that both CeO_2-D and CeO_2-P calcined at 500 °C have higher activities than those calcined at other temperatures. However, their activities are still much lower than that of flowerlike CeO_2 microspheres (Figure 11). The $T_{10\%}$ values of CeO_2 (500)-D and CeO_2 (500)-P are 129 and 151 °C, respectively, and their $T_{90\%}$ values are almost the same value of 225 °C.

CeO_2 is widely used in the catalytic oxidation reactions because of its unique properties such as high oxygen storage capacity (OSC) and the facile redox behaviors. Herein, hydrogen temperature programmed reduction (H_2-TPR) was used to test the reduction behavior of CeO_2. In the H_2-TPR curve of flowerlike CeO_2 microspheres (Figure 12a), there are two low-temperature reduction peaks centered at 358 and 483 °C, assigned to a reduction of surface capping oxygen species of CeO_2 (45), which are generally considered as the active oxygen in the low-temperature oxidations. The temperatures of these two low-temperature reduction peaks are evidently lower than those of both CeO_2 (500)-D and CeO_2 (500)-P, which are 400 and 515 °C, respectively (Figure 12b, c), whereas the three CeO_2 samples show another large peaks centered at the temperatures of ~810 °C, which is attributed to the reduction of bulk oxygen that

Table 2. Textural Properties of CeO_2 Samples and Their Amount of Hydrogen Consumed in H_2-TPR

sample	surface area ($m^2\ g^{-1}$)	pore volume ($cm^3\ g^{-1}$)	pore diameter (nm)	crystalline size (nm)	consumed H_2 ($\mu mol\ g^{-1}$)
CeO_2—F	181.4	0.20	3.9	6.5	589[a]
CeO_2(500)-D	76.3	0.23	10.6	10.6	343[b]
CeO_2(500)-P	42.7	0.12	12.8	15.7	328[c]
CeO_2—F (used)	181.3	0.20	3.9	6.5	351[d]

[a] Calculated from room temperature to 564 °C. [b] Calculated from room temperature to 648 °C. [c] Calculated from room temperature to 591 °C. [d] Calculated from room temperature to 570 °C.

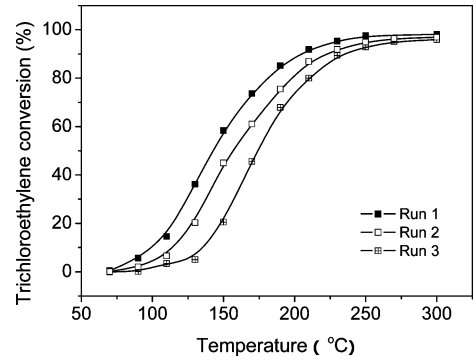

FIGURE 13. Light-off curves of catalytic combustion of trichloroethylene in three consecutive runs over CeO_2-F.

has no contribution to trichloroethylene combustion. In addition, the amount of hydrogen consumed by the surface capping oxygen in H_2-TPR process for flowerlike CeO_2 microspheres is more than that for CeO_2(500)-D and CeO_2(500)-P (Table 2). The lower reduction temperatures and larger hydrogen consumption of flowerlike CeO_2 microspheres compared with bulk CeO_2 indicate their higher oxygen mobility and more surface-active oxygen, which should be mainly attributed to their higher surface area and unique mesoporous structure that is favorable for gas diffusion inside flowerlike CeO_2 microspheres. Therefore, flowerlike CeO_2 microspheres performed higher activity in the trichloroethylene elimination than bulk CeO_2.

The stability test was also investigated. The results in Figure 13 show flowerlike CeO_2 microspheres deactivated gradually during the reaction. After three runs, $T_{90\%}$ declined to 235 °C. By EDS analysis, new Cl species are observed on the surface of flowerlike CeO_2 microspheres (Figure 14), suggesting that Cl_2 and HCl produced from trichloroethylene destruction were adsorbed on the surface of CeO_2 (33). In the H_2-TPR curve of used CeO_2-F (Figure 12d), the first reduction peak at 358 °C for fresh flowerlike CeO_2 microspheres disappears and the second reduction peak at 483 °C has been shifted to the higher temperature of 498 °C. The amount of hydrogen consumed by the surface active oxygen is also decreased, whereas the BET surface area is unchanged (Table 2). Therefore, it can be considered that chlorine with high electronegativity has occupied oxygen vacancies which were generally formed by surface oxygen consumption in trichloroethylene combustion, resulting in a hard recovery of the surface active oxygen from gas oxygen or bulk oxygen, so the flowerlike CeO_2 microspheres were deactivated gradually during the reaction. Likewise, the

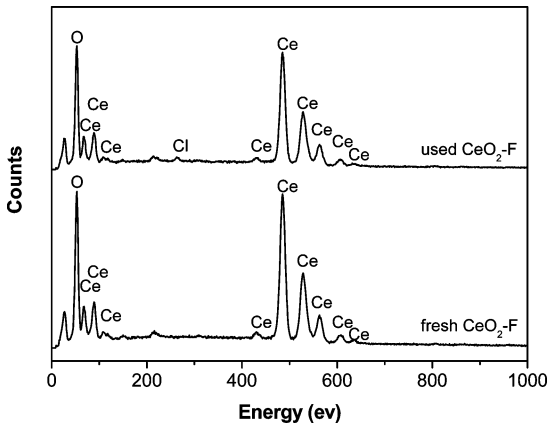

FIGURE 14. EDS analysis of fresh and used CeO_2-F.

deactivation of bulk CeO_2 resulting from Cl poisoning has also been testified. Till now, the deactivation of metal-based catalysts caused by Cl species produced in CVOC combustion is a general phenomenon and how to improve their stability is still an important subject in this research field (46, 47). In our later work, we have found that doping other metal cations such as Mn cations into flowerlike CeO_2 microspheres to form high surface area ceria-based composite oxides can obviously improve their stability and also significantly enhance their activity in the trichloroethylene combustion. More detailed work will be published as a monograph.

4. CONCLUSION

In summary, various hydrothermal routes were adopted to successfully prepare flowerlike $Ce(OH)CO_3$ microspheres and further CeO_2 microspheres after calcination. These flowerlike CeO_2 microspheres, especially prepared in the glucose/acrylic acid system, have very high surface area, uniform mesopore structure and large pore volume. As for the formation mechanism of flowerlike $Ce(OH)CO_3$ microspheres, it is proposed that the in situ produced large N-containing organic compounds were mainly responsible for controlling assembly of $Ce(OH)CO_3$ building blocks into the flowerlike $Ce(OH)CO_3$ microspheres. In addition, more and larger N-containing organic compounds produced by the decomposition of graft-copolymers formed in glucose/acrylic acid or fructose/acrylic acid systems were favorable for increasing the surface areas of flowerlike CeO_2 microspheres by promoting the production of mesostructures. The flowerlike CeO_2 microspheres exhibited much higher catalytic activity in catalytic combustion of trichloroethylene than general CeO_2, attributed to their high oxygen mobility and rich surface-active oxygen resulting from high surface area and unique mesostructure.

Acknowledgment. This work was supported financially by the National Basic Research Program of China (2004CB719500), the National Natural Science Foundation of China (20673037), and the Commission of Science and Technology of Shanghai Municipality (06JC14095).

Supporting Information Available: Figures S1−S3 include a SEM image of one bird's-nest-like CeO_2 hollow microsphere prepared in the glucose/acrylic acid system, the XRD patterns of $Ce(OH)CO_3$ microspheres prepared in the glucose/propanoic acid system, and the GC-MS spectra of organic products after hydrothermal reaction in the glucose/acrylic acid and glucose/propanoic acid systems, respectively (PDF). This material is available free of charge via the Internet at http://pubs.acs.org.

REFERENCES AND NOTES

(1) Trovarelli, A. *Catal. Rev. Sci. Eng.* **1996**, *38*, 439–520.
(2) Reddy, B. M.; Bharali, P.; Saikia, P. *J. Phys. Chem. C* **2007**, *111*, 1878–1881.
(3) Park, S. D.; Vohs, J. M.; Gorte, R. J. *Nature* **2000**, *404*, 265–267.
(4) Beie, H. J.; Gnoerich, A. *Sens. Actuators B* **1991**, *4*, 393–399.
(5) Yu, X. J.; Xie, P. B.; Su, Q. D. *Phys. Chem. Chem. Phys.* **2001**, *3*, 5266–5269.
(6) Shchukin, D. G.; Carus, R. A. *Chem. Mater.* **2004**, *16*, 2287–2292.
(7) Sohlberg, K.; Pantelides, S. T.; Pennycook, S. F. *J. Am. Chem. Soc.* **2001**, *123*, 6609–6611.
(8) Wang, S.; Lu, G. Q. *Appl. Catal. B: Environ.* **1998**, *19*, 267—277.
(9) Ho, C. M.; Yu, J. C.; Kwong, T.; Mak, A. C.; Lai, S. *Chem. Mater.* **2005**, *17*, 4514–4522.
(10) Ji, P. F.; Zhang, J. L.; Chen, F.; Anpo, M. *J. Phys. Chem. C* **2008**, *112*, 17809–17813.
(11) Liao, L.; Mai, H. X.; Yuan, Q.; Lu, H. B.; Li, J. C.; Liu, C.; Yan, C. H. *J. Phys. Chem. C* **2008**, *112*, 9061–9065.
(12) Du, N.; Zhang, H.; Chen, B. D.; Ma, X. Y.; Yang, D. R. *J. Phys. Chem. C* **2007**, *111*, 12677–12680.
(13) Han, W. Q.; Wu, L. J.; Zhu, Y. M. *J. Am. Chem. Soc.* **2005**, *127*, 12814–12815.
(14) Yang, S. W.; Gao, L. *J. Am. Chem. Soc.* **2006**, *128*, 9330–9331.
(15) Si, R.; Zhang, Y. W.; You, L. P.; Yan, C. H. *Angew. Chem., Int. Ed.* **2005**, *44*, 3256–3260.
(16) Zhou, H. P.; Zhang, Y. W.; Mai, H. X.; Sun, X.; Liu, Q.; Song, W. G.; Yan, C. H. *Chem.—Eur. J.* **2008**, *14*, 3380–3390.
(17) Shen, W. H.; Dong, X. P.; Zhu, Y. F.; Chen, H. R.; Shi, J. L. *Microporous Mesoporous Mater.* **2005**, *85*, 157–162.
(18) Zhou, K. B.; Yang, Z. Q.; Yang, S. *Chem. Mater.* **2007**, *19*, 1215–1217.
(19) Zhou, H. P.; Zhang, Y. W.; Si, R.; Zhang, L. S.; Song, W. G.; Yan, C. H. *J. Phys. Chem. C* **2008**, *112*, 20366–20376.
(20) Mai, H. X.; Sun, L. D.; Zhang, Y. W.; Si, R.; Feng, W.; Zhang, H. P.; Liu, H. C.; Yan, C. H. *J. Phys. Chem. B* **2005**, *109*, 24380—24385.
(21) Feng, X. D.; Sayle, D. C.; Wang, Z. L.; Paras, M. S.; Santora, B.; Sutorik, A. C.; Sayle, T. X. T.; Yang, Y.; Ding, Y.; Wang, X. D.; Her, Y. S. *Science* **2006**, *312*, 1504–1508.
(22) Kuiry, S. C.; Patil, S. D.; Deshpande, S.; Seal, S. *J. Phys. Chem. B* **2005**, *109*, 6936–6939.
(23) Liao, X. H.; Zhu, J. M.; Zhu, J. J.; Xu, J. Z.; Chen, H. Y. *Chem.Commun.* **2001**, 937–938.
(24) Li, Z. X.; Li, L. L.; Yuan, Q.; Feng, W.; Xu, J.; Sun, L. D.; Song, W. G.; Yan, C. H. *J. Phys. Chem. C* **2008**, *112* (47), 18405–18411.
(25) Pan, C. S.; Zhang, D. S.; Shi, L. Y.; Fang, J. H. *Eur. J. Inorg. Chem.* **2008**, 2429–2436.
(26) Cao, M. H.; Liu, T. F.; Gao, S.; Sun, G. B.; Wu, X. L.; Hu, C. W.; Wang, Z. L. *Angew. Chem., Int. Ed.* **2005**, *44*, 4197–4201.
(27) Zhang, S. M.; Zeng, H. C. *Chem. Mater.* **2009**, *21* (5), 871–883.
(28) Zhong, L. S.; Hu, J. S.; Cao, A. M.; Liu, Q.; Song, W. G.; Wan, L. J. *Chem. Mater.* **2007**, *19*, 1648–1655.
(29) Sun, C. W.; Sun, J.; Xiao, G. L.; Zhang, H. R.; Qiu, X. P.; Li, H.; Chen, L. Q. *J. Phys. Chem. B* **2006**, *110*, 13445–13452.
(30) Wang, S. R.; Zhang, J.; Jiang, J. Q.; Liu, R.; Zhu, B. L.; Xu, M. J.; Wang, Y.; Cao, J. L.; Li, M. Y.; Yuan, Z. Y.; Zhang, S. M.; Huang, W. P.; Wu, S. H. *Microporous Mesoporous Mater.* **2009**, *123*, 349–353.
(31) Kim, O. K.; Griffith, J. R. *J. Polym. Sci., Part A: Polym. Chem.* **1975**, *13*, 151–160.
(32) Mishra, S.; Panda, A.; Singh, B. C. *J. Appl. Polym. Sci.* **1999**, *73*, 677–683.
(33) Dai, Q. G.; Wang, X. Y.; Lu, G. Z.*Catal. Commun.* **2007**, *8*, 1645–1649.
(34) Orth, W. S.; Gillham, R. W.*Environ. Sci. Technol.* **1996**, *30*, 66–71.
(35) Lin, C. J.; Lo, S. L.; Liou, Y. H.*J. Hazard. Mater.* **2004**, *116*, 219–228.

(36) González-Velasco, J. R.; Aranzabal, A.; López-Fonseca, R.; Ferret, R.; González-Marcos, J. R. *Appl. Catal., B: Environ.* **2000**, *24*, 33–43.
(37) López-Fonseca, R.; Aranzabal, A.; Álvarez-Uriarte, J. I.; González-Velasco, J. R. *Appl. Catal., B: Environ.* **2001**, *30*, 303–313.
(38) McKeown, N. B.; Budd, P. M.; Msayib, K. J.; Ghanem, B. S.; Kingston, H. J.; Tattershall, C. E.; Makhseed, S.; Reynolds, K. J.; Fritsch, D. *Chem.—Eur. J.* **2005**, *11*, 2610–2620.
(39) Meng, Y.; Gu, D.; Zhang, F. Q.; Shi, Y. F.; Cheng, L.; Feng, D.; Wu, Z. X.; Chen, Z. X.; Wan, Y.; Stein, A.; Zhao, D. Y. *Chem. Mater.* **2006**, *18*, 4447–4464.
(40) Ellis, A. V.; Wilson, M. A. *J. Org. Chem.* **2002**, *67*, 8469–8474.
(41) Yang, B. Y.; Montgomery, R. *Carbohydr. Res.* **1996**, *280*, 27—45.
(42) Robeson, L. M.; Kuphal, J. A.; Vratsanos, M. S. *J. Appl. Polym. Sci.* **1996**, *61*, 1561–1569.
(43) Colfen, H.; Mann, S. *Angew. Chem., Int. Ed.* **2003**, *42*, 2350–2365.
(44) Zhang, X. J.; Ma, T. Y.; Yuan, Z. Y. *Eur. J. Inorg. Chem.* **2008**, 2721–2726.
(45) Concepcion, P.; Corma, A.; Silvestre-Albero, J.; Franco, V.; Chane-Ching, J. Y. *J. Am. Chem. Soc.* **2004**, *126*, 5523–5532.
(46) Imamura, S. *Catal. Today.* **1992**, *11*, 547–567.
(47) Mishra, T.; Mohapatra, P.; Parida, K. M. *Appl. Catal., B: Environ.* **2008**, *79*, 279–285.

AM900829Y